Supplement of Atmos. Chem. Phys., 26, 12813–12836, 2026
https://doi.org/10.5194/acp-26-12813-2026-supplement

Atmospheric Chemistry and Physics
Open Access
EGU

Supplement of

Unraveling the chemical structures and sources of biomass-derived organic aerosols through a year-long offline analysis in Hyytiälä, Finland

Qianzhe Sun et al.

Correspondence to: Michihiro Mochida (mochida@isee.nagoya-u.ac.jp)

Text S1 Quantification of organic matter by the least squares method

In the case that all quantified fragment ions are used for the least squares method, five ions (m/z 28, 44, 50, 76, and 104) deviate significantly from the regression line for some samples with low concentrations. Because of their high signal intensities, these ions could substantially affect the overall fitting result. To assess the influence of different ion exclusion methods on the quantification of WSOM, WSOC from the AMS analysis (WSOM divided by OM/OC) was compared with that from the TOC analysis with the following four methods: S1, excluding m/z 28 and 44; S2, excluding m/z 50, 76, and 104; S3, excluding all five ions; and S4, with no ions excluded. As shown in Figure S1, the method in which all five ions were excluded (S3) yielded a higher Pearson correlation coefficient between WSOC from AMS and the TOC analyzer (r = 0.99) than any other method (r = 0.97). In addition, compared with the slope of other methods (0.89–0.95), S3 exhibited the slope closest to unity (0.99). For these reasons, the exclusion of all five ions was adopted for the quantification of WSOM in this study.

Text S2 Calculation of particle volume concentration from DMPS-derived size distributions

Particle number size distributions $dN/d\log D_p$ in the diameter range of 100–1000 nm, where N and D_p denote particle number concentration and particle diameter, respectively, were obtained from the differential mobility particle sizer (DMPS) instrument at the Hyytiälä forest station (the data are available at the SmartSMEAR online platform: https://smear.avaa.csc.fi). The DMPS measurement provides size-resolved particle number concentrations by classifying particles according to their electrical mobility. The $dN/d\log D_p$ (cm^{-3}) for 21 diameters ($D_{p,i}$, i = 1, 2, ..., 21, from small to large diameters) were used to calculate particle volume concentrations. Except for $D_{p,1}$ and $D_{p,21}$, the $D_{p,i}$ were considered as the geometric mean diameters of consecutive size bins, and the lower and upper ends of the bin corresponding to $D_{p,i}$, $D_{p,lower}$ and $D_{p,upper,i}$, respectively, were determined by assuming logarithmically equal spacing between adjacent DMPS diameters:

$$D_{p,lower,i} = \sqrt{D_{p,i-1} D_{p,i}}, \quad D_{p,upper,i} = \sqrt{D_{p,i} D_{p,i+1}} \tag{S1}$$

$D_{p,lower,1}$ and $D_{p,upper,21}$ were set to 100 and 1000 (nm), respectively.

The particle volume concentration for the bin corresponding to $D_{p,i}$ (V_i, $\mu m^3\ cm^{-3}$) was calculated as follows:

$$V_i = \frac{\pi}{6} D_{p,i}^3 \cdot \frac{dN}{d\log D_{p,i}} \cdot (\log D_{p,upper,i} - \log D_{p,lower,i}) \tag{S2}$$

The total volume concentration was calculated as the sum of V_i over all bins within the selected size range.

Text S3 Selection of the PMF factor solution

PMF solutions with different numbers of factors were tested for the analysis in this study. Two and three factor solutions were not used because the $Q/Q_{expected}$ values are substantially higher than the cases of four and five factor solutions. The PMF results from a four factor solution provided interpretable source apportionment and were broadly consistent with previous studies summarized in Table 1, such as Crippa et al. (2014). Both the four and five factor solutions were considered to provide reasonable source interpretations.

Although $Q/Q_{expected}$ continues to decrease with increasing factor number, the improvement becomes minor after the five factor solution (Fig. S4d). As shown in Fig. S4g, increasing the number of factors to six or seven does not substantially change the dominant temporal patterns or the distributions of the major factors among the three OA fractions compared with the five-factor solution. The main changes are considered to be factor splitting or addition of minor factors as explained below.

In the six-factor solution, both the mass-concentration time series and the spectral profiles of F1, F2, F3, F4, and F6 (where F*i* denotes factor *i*, *i* = 1, 2, 3, ...) closely resemble those of F1, F2, F3, F4, and F5, respectively, in the five-factor solution. For each factor in the five-factor solution, its corresponding factor in the six-factor solution shows the highest correlation on a mass-concentration basis ($r > 0.938$) and the highest mass-spectral correlation ($r > 0.996$) among all possible factor pairings, and a similar annual mean mass contribution (91.9–101.4% of that of the corresponding factor in the five-factor solution). Factor F5 in the six-factor solution accounted for only 4.4% of the total reconstructed OA concentration on average, indicating that this additional factor had a limited influence on the overall mass budget. The factor profile of F5 in the six-factor solution was dominated by low-m/z fragments, with a particularly strong signal at m/z 29. This mass spectral pattern is not similar to common mass spectral patterns associated with a specific source in conventional AMS analysis. Therefore, the six-factor solution was not selected for further analysis. It should be noted, however, that F5 should not be considered meaningless solely on the basis of its mass spectral pattern, because a PMF factor may represent a group of molecular substructures rather than a group of intact compounds. The abundance of CHN-family ions (5.2%) suggests that F5 is related to a specific type of BBOA, although this relationship cannot be conclusively established.

In the case of the seven-factor solution, F4 is similar to F5 in the six-factor solution, with the highest correlation on a mass-concentration basis ($r = 0.963$) and the highest mass-spectral correlation ($r = 0.988$) among all possible factor pairings. Hence, as in the case of F5 in the six-factor solution, F4 cannot be clearly associated with a known source. F1, F2, F3, F6, and F4 in the seven-factor solution correspond most closely to F1, F2, F3, F4, and F5, respectively, in the six-factor solution, showing the highest mass-concentration correlations ($r > 0.917$) and the highest mass-spectral correlations ($r > 0.982$) among all possible individual-factor pairings, as well as similar annual mean mass contributions (81.7–121.8% of those of the corresponding factors in the six-factor solution). The sum of F5 and F7 in the seven-factor solution showed the highest mass-concentration correlation with F6 among all factors in the six-factor solution ($r = 0.997$) and had a similar mean fractional contribution (112.8% of that of F6 in the six-factor solution). Further, the O/C ratios of six-factor F6 and seven-factor F5 and F7 were 0.15, 0.16, and 0.20, respectively, all of which were relatively low and comparable to that of HOA in the five-factor solution (O/C = 0.15). Taken together, we considered F6 in the six-factor solution to be mainly split into F5 and F7 in the seven-factor solution; the two split factors cannot be explicitly attributed to different known sources. For the reasons above, the seven-factor solution was not selected for further analysis.

Overall, these results indicate that although the six- and seven-factor solutions increased the number of resolved factors, they did not substantially change the source-apportionment interpretation compared with the five-factor solution. The five-factor solution was selected as a conservative solution because the number of resolved factors was close to those reported in previous PMF studies at Hyytiälä (Table 1). Although higher-factor solutions may contain more information on submolecular structures or mixed sources, their source interpretation remains a challenge. The five-factor solution was therefore used for further discussion in the present study.

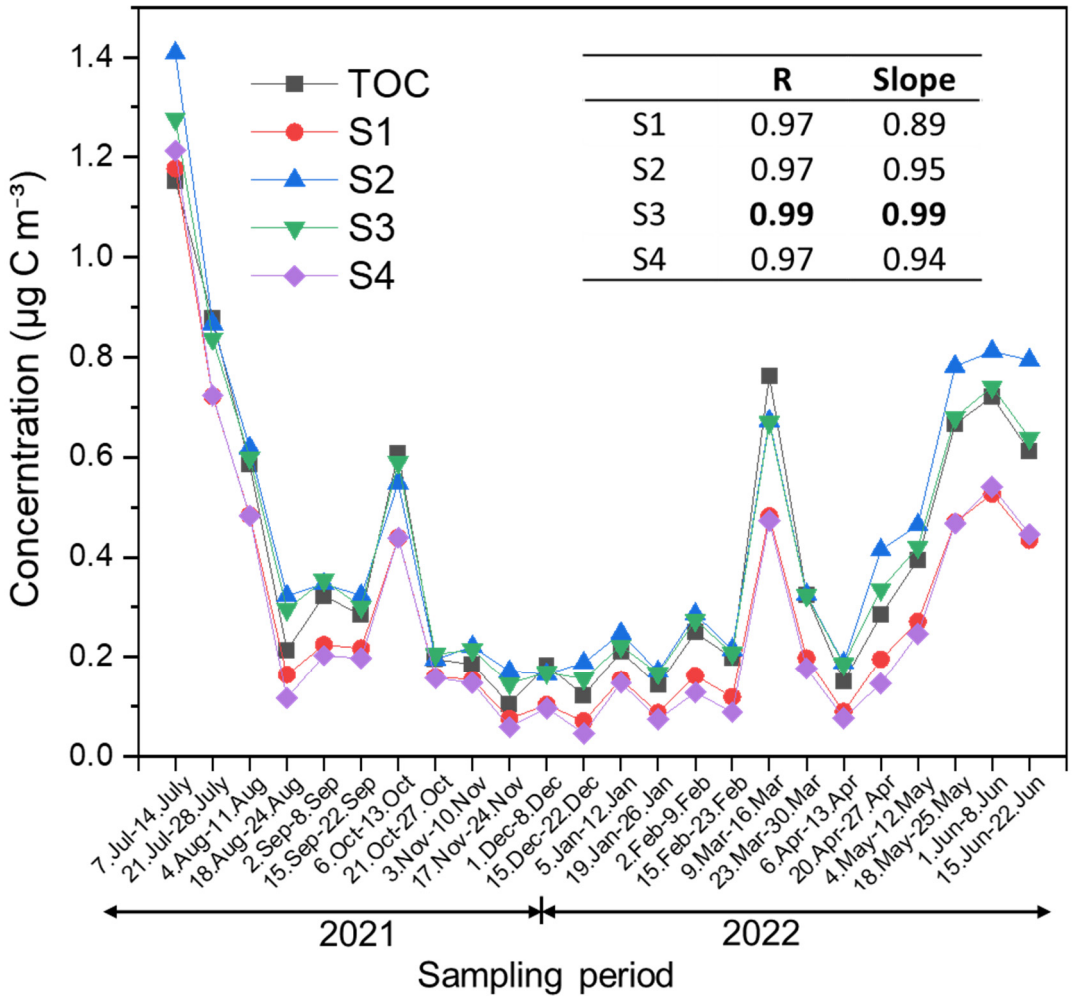

Figure S1. Comparison of WSOC concentrations derived from AMS using different fragment ion screening methods with those from TOC measurements.

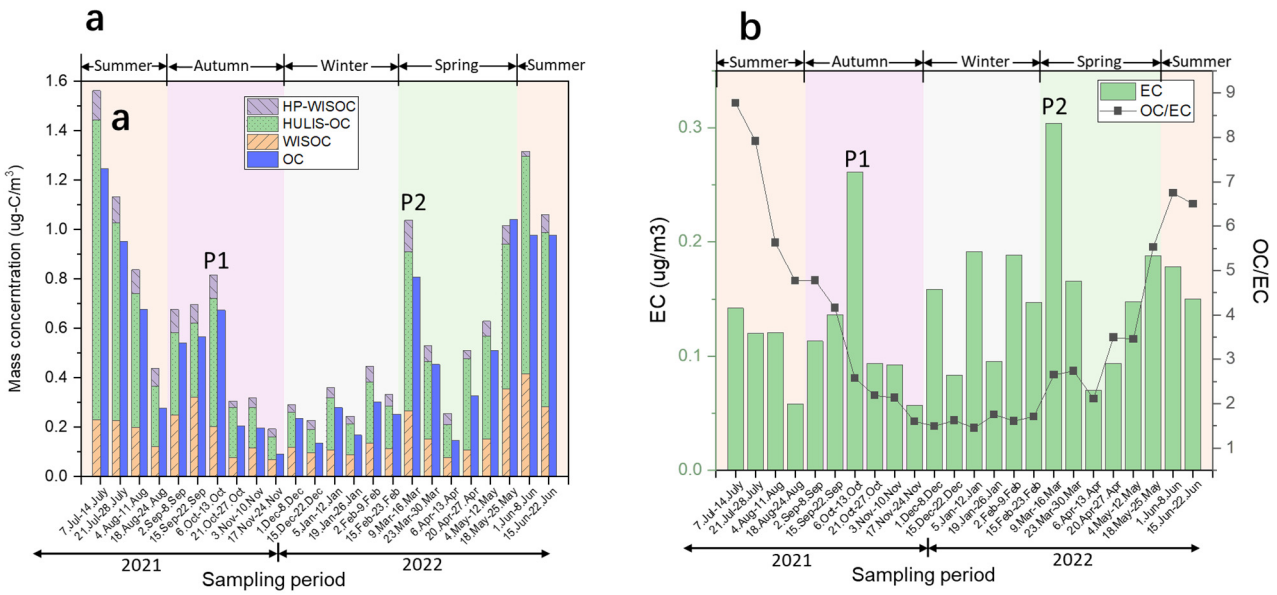

Figure S2. (a) Seasonal variations in the carbon concentrations of the HP-WSOM, HULIS, and WISOM fractions (HP-WISOC, HULIS-OC, and WISOC, respectively), and the concentrations of OC from the thermal/optical carbon analysis.. (b) The variations in the concentrations of EC and the OC/EC ratios.

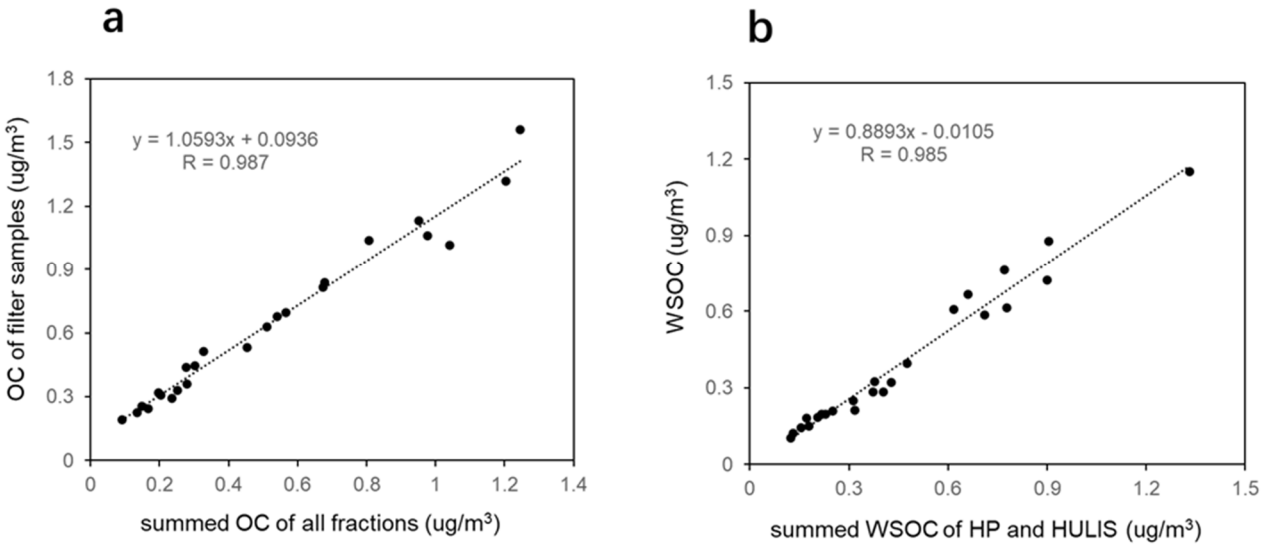

Figure S3. (a) Scatter plot of the summed OC derived from the carbon analyzer and that from AMS. (b) Scatter plot of the WSOC derived from the TOC analyzer and the sum of carbon in HP-WSOM and HULIS from the AMS. The dotted lines represent regression lines, and the equations of the lines and correlation coefficients (*r*) are also presented.

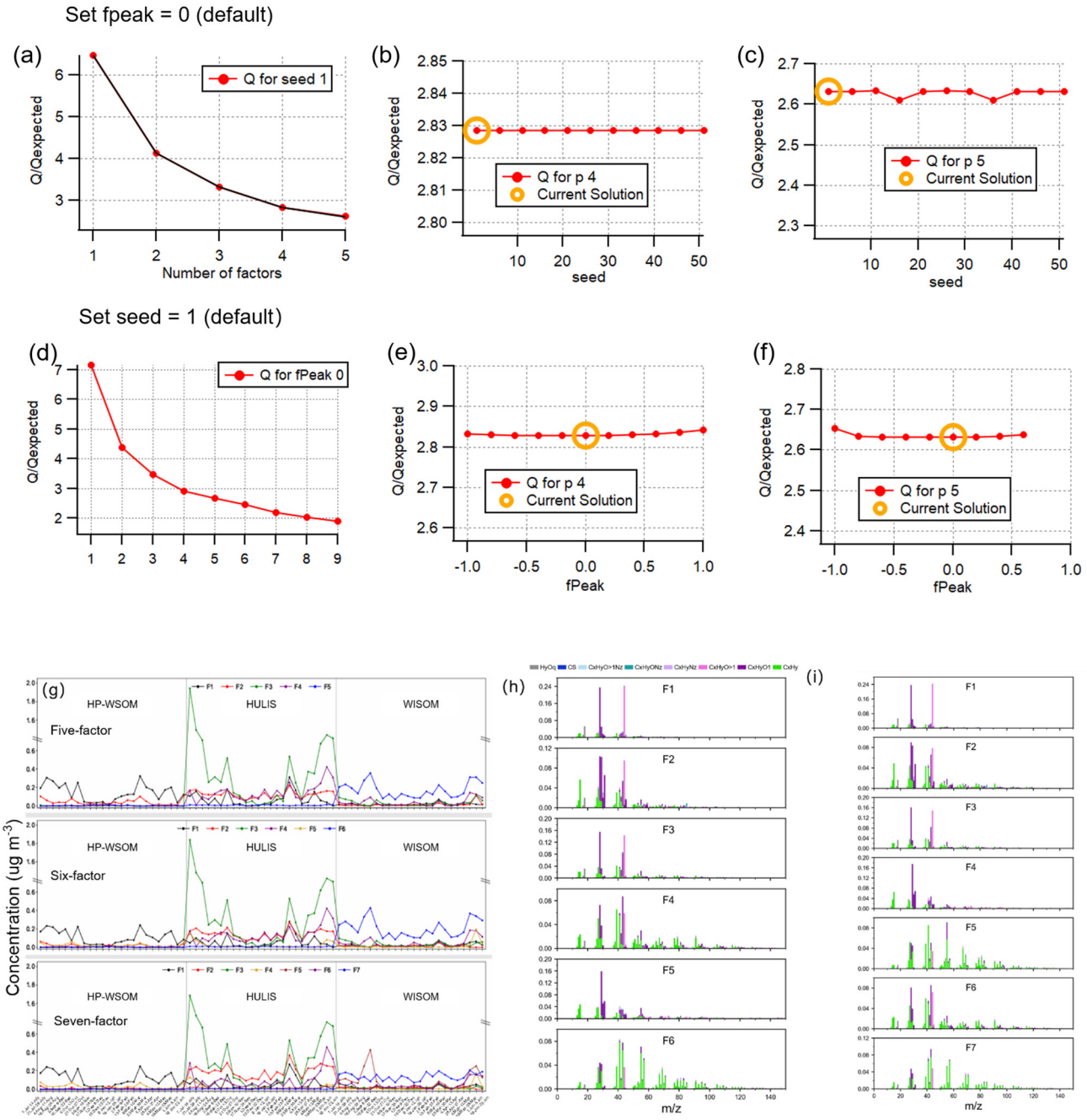

Figure S4. Evaluation of the PMF solutions using $Q/Q_{expected}$ as a function of the number of factors, seed values, and fPeak values: (a) $Q/Q_{expected}$ as a function of the number of factors for seed = 1; (b) $Q/Q_{expected}$ as a function of seed for the 4-factor solution; (c) $Q/Q_{expected}$ as a function of seed for the 5-factor solution; (d) $Q/Q_{expected}$ as a function of the number of factors for fPeak = 0; (e) $Q/Q_{expected}$ as a function of fPeak for the 4-factor solution; (f) $Q/Q_{expected}$ as a function of fPeak for the 5-factor solution; (g) Quantified concentration time series for the five-, six-, and seven-factor PMF solutions across HP-WSOM, HULIS, and WISOM fractions. The y-axis is broken to highlight both the dominant peaks and low-amplitude variations; (h) Factor mass spectral profiles for the six-factor PMF solution; (i) Factor mass spectral profiles for the seven-factor PMF solution. In panels g–i, F*i* denotes factor *i* (*i* = 1, 2, 3, ...).

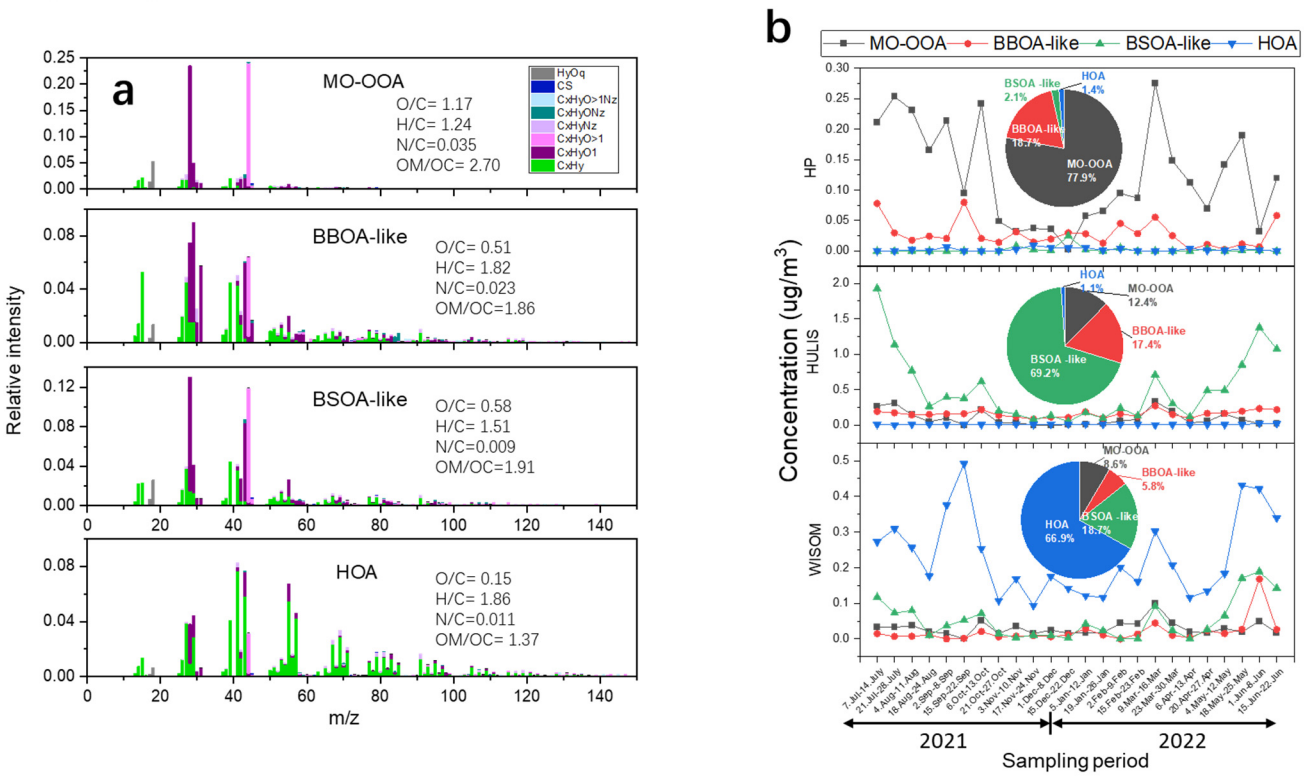

Figure S5. (a) HR–AMS spectra of the PMF factors from the four-factor solution and results from the elemental analysis. (b) Time series and mean contributions of MO-OOA, BBOA-like, BSOA-like, and HOA factors in HP-WSOM, HULIS and WISOM.

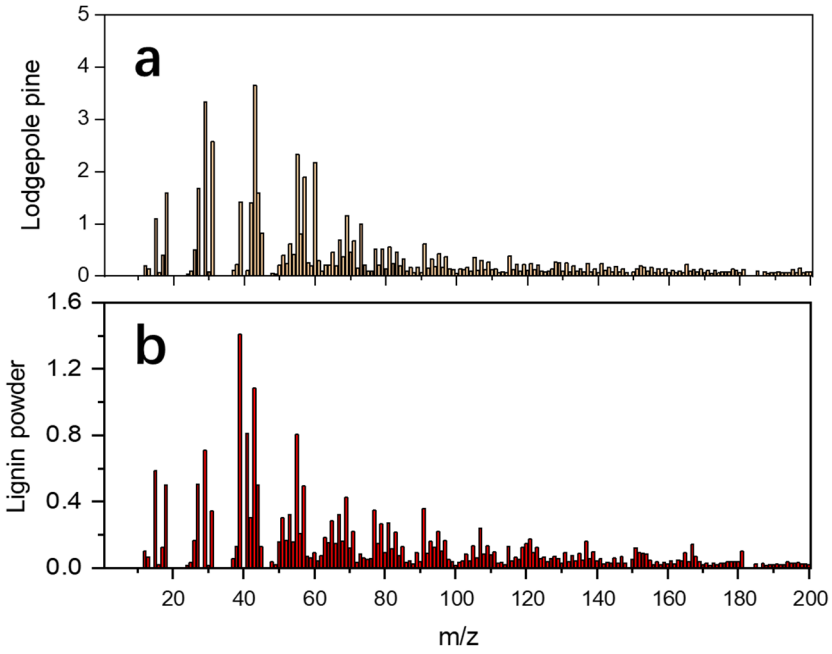

Figure S6. (a) Reference spectra of (a) lodgepole pine and (b) lignin powder, both retrieved from the AMS spectral database (Ulbrich et al., 2009; Ulbrich).

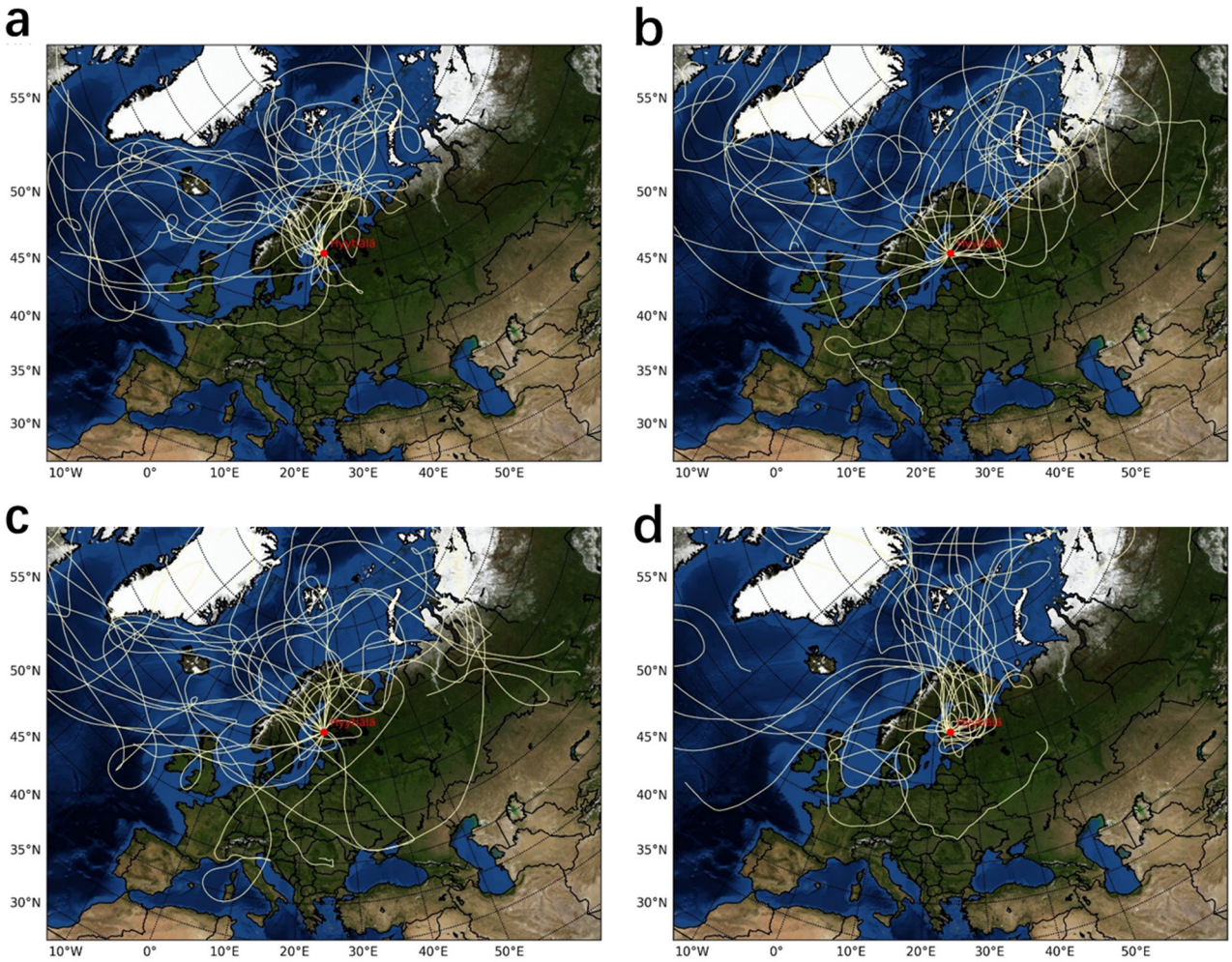

Figure S7. Five-day backward air mass trajectories for (a) summer, (b) autumn, (c) winter, and (d) spring. Some parts of the trajectories extend beyond the displayed map domain.

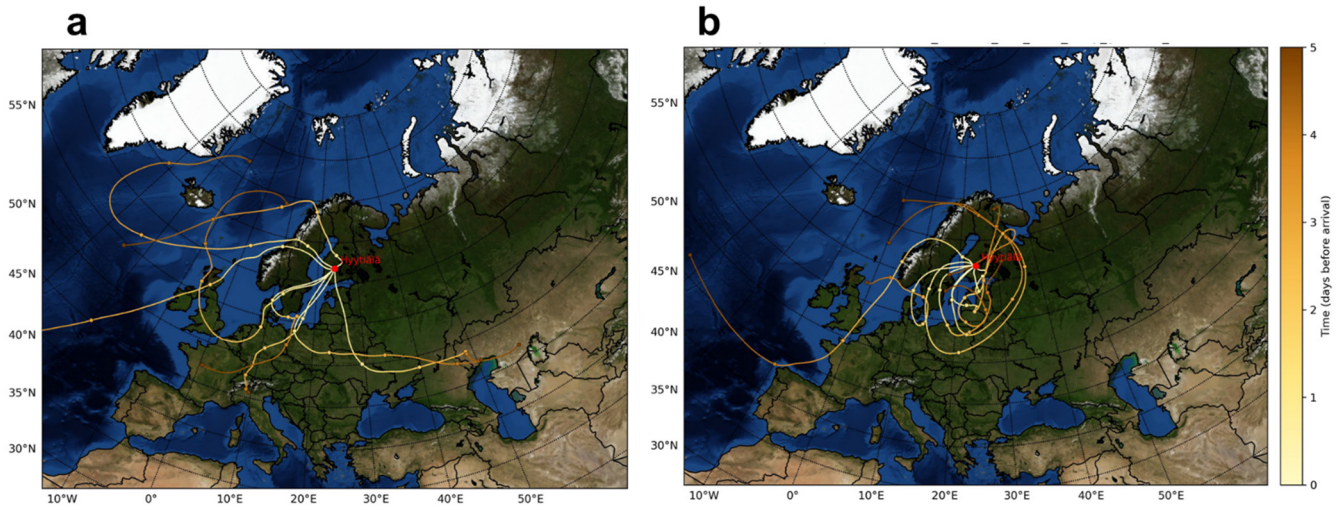

Figure S8. Five-day backward air mass trajectories during periods P1 (a) and P2 (b), colored by transport time. The dots on the trajectories indicate daily intervals, and their colors correspond to the transport time shown by the color scale. Part of a trajectory is outside the map domain.

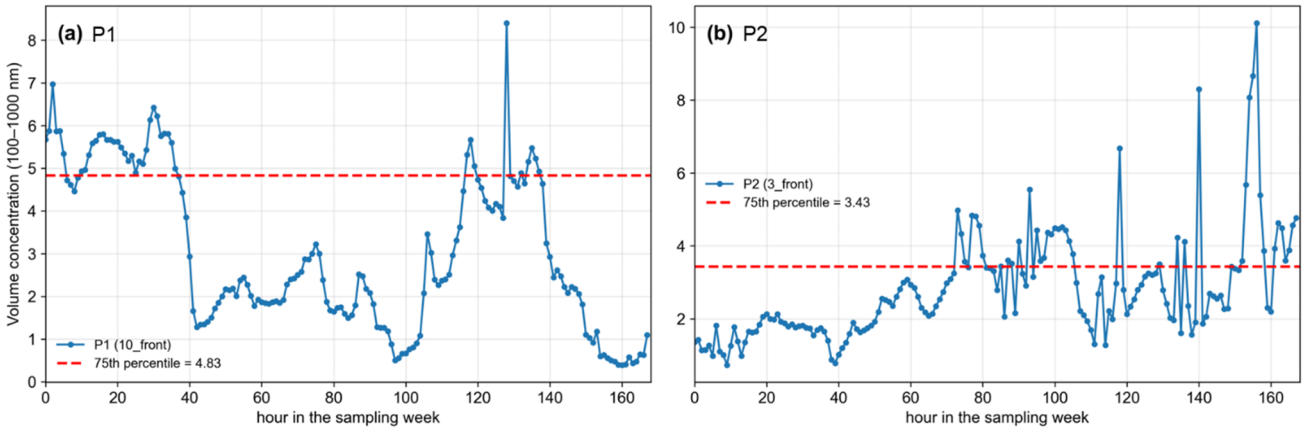

Figure S9. The volume concentrations for the 100–1000 nm size range during the sampling week for (a) P1 and (b) P2 (blue markers), and the 75th percentile thresholds for selecting high concentration hours in the PSCF analysis (red dashed lines).

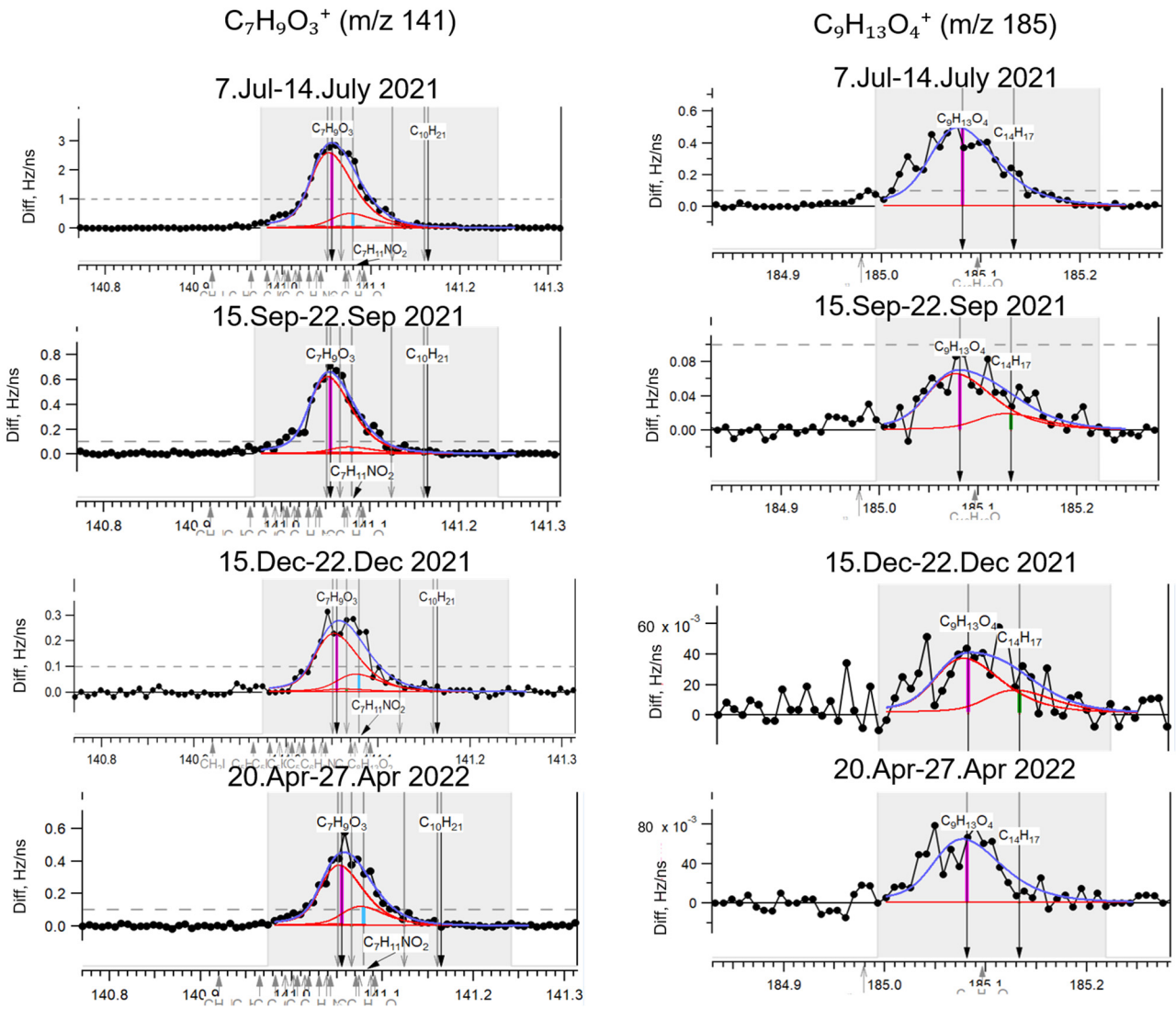

Figure S10. Examples of HR peak-fittings for $C_7H_9O_3^+$ and $C_9H_{13}O_4^+$ ions for the HULIS fraction. Four samples collected in summer, autumn, winter, and spring are selected.

Table S1. Sample information.

Sample ID	Sampling start time (UTC+2)	Sampling end time (UTC+2)	Duration (h)	Sampled air volume (m^3)
FIN20QFF002	14:33, 7 Jul, 2021	12:16, 14 Jul, 2021	166	11471.3
FIN20QFF004	14:10, 21 Jul, 2021	8:11, 28 Jul, 2021	162	11192.1
FIN20QFF006	8:33, 4 Aug, 2021	6:53, 11 Aug, 2021	166	11464.1
FIN20QFF009	11:40, 18 Aug, 2021	13:14, 24 Aug, 2021	146	9996.2
FIN20QFF011	14:48, 2 Sep, 2021	13:07, 8 Sep, 2021	142	9847.5
FIN20QFF014	11:36, 15 Sep, 2021	12:29, 22 Sep, 2021	169	11659.5
FIN20QFF018	12:58, 6 Oct, 2021	13:25, 13 Oct, 2021	168	11662.5
FIN20QFF021	14:59, 21 Oct, 2021	12:27, 27 Oct, 2021	141	9745.4
FIN20QFF023	14:40, 3 Nov, 2021	13:53, 10 Nov, 2021	167	11509.6
FIN20QFF026	15:01, 17 Nov, 2021	13:35, 24 Nov, 2021	167	11434.1
FIN20QFF028	14:59, 1 Dec, 2021	14:13, 8 Dec, 2021	167	11495.7
FIN20QFF031	15:59, 15 Dec, 2021	14:05, 22 Dec, 2021	166	11440.1
FIN20QFF034	11:04, 5 Jan, 2022	10:03, 12 Jan, 2022	167	11458.9
FIN20QFF037	14:46, 19 Jan, 2022	13:45, 26 Jan, 2022	167	11514.9
FIN20QFF039	15:59, 2 Feb, 2022	13:53, 9 Feb, 2022	166	11431.1
FIN20QFF042	15:56, 15 Feb, 2022	14:34, 23 Feb, 2022	191	13139
FIN20QFF046	10:48, 9 Mar, 2022	14:38, 16 Mar, 2022	172	11883.8
FIN20QFF048	13:22, 23 Mar, 2022	13:21, 30 Mar, 2022	168	11608.8
FIN22QFF002	14:31, 6 Apr, 2022	12:57, 13 Apr, 2022	166	11517.4
FIN22QFF004	14:50, 20 Apr, 2022	13:06, 27 Apr, 2022	166	11465.2
FIN22QFF007	15:43, 4 May, 2022	13:45, 12 May, 2022	190	13123
FIN22QFF009	13:51, 18 May, 2022	12:37, 25 May, 2022	167	11561.1
FIN22QFF012	14:58, 1 Jun, 2022	13:14, 8 Jun, 2022	166	11472.5
FIN22QFF014	7:50, 15 Jun, 2022	13:29, 22 Jun, 2022	174	11994.7

Table S2. Extraction efficiency of samples using the SPE technique. All concentration data shown in this table have been converted to atmospheric concentrations and were obtained from offline HR-AMS measurements and quantified using the phthalic acid internal standard method.

Sample ID	Organic matter ($\mu g\ m^{-3}$)			SPE extraction efficiency (%)
	WSOM	HULIS	HP-WSOM	
FIN20QFF002	2.52	2.40	0.31	107.2%
FIN20QFF004	1.71	1.63	0.37	116.8%
FIN20QFF006	1.15	1.07	0.30	119.8%
FIN20QFF009	0.58	0.48	0.24	123.6%
FIN20QFF011	0.70	0.66	0.29	136.5%
FIN20QFF014	0.56	0.56	0.18	129.9%
FIN20QFF018	1.17	1.06	0.29	115.1%
FIN20QFF021	0.39	0.39	0.06	114.1%
FIN20QFF023	0.41	0.32	0.09	98.0%
FIN20QFF026	0.27	0.17	0.06	86.3%
FIN20QFF028	0.31	0.26	0.09	112.5%
FIN20QFF031	0.28	0.18	0.06	84.0%
FIN20QFF034	0.41	0.39	0.13	125.9%
FIN20QFF037	0.31	0.23	0.13	115.8%
FIN20QFF039	0.53	0.48	0.21	130.1%
FIN20QFF042	0.42	0.34	0.18	126.1%
FIN20QFF046	1.38	1.32	0.43	126.9%
FIN20QFF048	0.67	0.65	0.25	134.6%
FIN22QFF002	0.36	0.26	0.19	124.9%
FIN22QFF004	0.65	0.71	0.10	125.1%
FIN22QFF007	0.83	0.82	0.18	120.8%
FIN22QFF009	1.31	1.13	0.23	103.7%
FIN22QFF012	1.40	1.66	0.05	122.4%
FIN22QFF014	1.20	1.33	0.23	129.8%

Table S3. Repeatability of the quantification of organic fractions.

	WSOM ($\mu g\ m^{-3}$)	WISOM ($\mu g\ m^{-3}$)	HP-WSOM ($\mu g\ m^{-3}$)	HULIS ($\mu g\ m^{-3}$)
FIN20QFF006_1st analysis	1.19	0.31	0.33	1.10
FIN20QFF006_2nd analysis	1.10	0.32	0.28	1.04
Difference	-7.7%	3.9%	-17.0%	-4.9%
FIN20QFF018_1st analysis	1.19	0.34	0.27	1.04
FIN20QFF018_2nd analysis	1.24	0.28	0.28	0.88
Difference	4.6%	-16.5%	1.8%	-15.4%

Table S4. Proportions of the mean mass contributions of the PMF factors of the four-factor solution (ug m^{-3}).

Sample ID	MO-OOA	BBOA	BSOA	HOA
FIN20QFF002	17.0%	9.3%	66.1%	7.6%
FIN20QFF004	28.5%	9.3%	51.1%	11.0%
FIN20QFF006	27.0%	10.3%	49.5%	13.2%
FIN20QFF009	30.5%	21.3%	30.7%	17.6%
FIN20QFF011	28.4%	14.0%	32.6%	25.0%
FIN20QFF014	8.4%	20.4%	35.8%	35.3%
FIN20QFF018	31.4%	15.5%	40.2%	12.9%
FIN20QFF021	16.6%	27.8%	37.6%	18.1%
FIN20QFF023	17.4%	27.6%	28.6%	26.4%
FIN20QFF026	15.5%	30.7%	25.1%	28.7%
FIN20QFF028	13.3%	27.7%	27.5%	31.5%
FIN20QFF031	5.9%	39.7%	19.9%	34.5%
FIN20QFF034	14.6%	36.3%	30.9%	18.2%
FIN20QFF037	28.8%	26.0%	23.5%	21.8%
FIN20QFF039	26.0%	25.2%	28.0%	20.8%
FIN20QFF042	35.5%	25.7%	18.5%	20.3%
FIN20QFF046	35.2%	17.5%	35.8%	11.5%
FIN20QFF048	39.2%	17.1%	28.1%	15.5%
FIN22QFF002	40.5%	18.6%	20.8%	20.1%
FIN22QFF004	14.9%	20.2%	52.6%	12.2%
FIN22QFF007	28.7%	14.7%	43.9%	12.7%
FIN22QFF009	15.9%	12.3%	52.4%	19.4%
FIN22QFF012	4.4%	15.9%	64.1%	15.6%
FIN22QFF014	9.5%	15.9%	59.6%	15.0%
Mean	17.0%	9.3%	66.1%	7.6%

Table S5. Proportions of the mean mass contributions of the PMF factors of the five-factor solution (μg m^{-3}).

Sample ID	MO-OOA	BBOA1	BSOA	BBOA2	HOA
FIN20QFF002	10.3%	9.2%	66.6%	6.7%	7.1%
FIN20QFF004	20.4%	10.4%	57.5%	1.4%	10.4%
FIN20QFF006	21.8%	9.7%	48.3%	7.8%	12.3%
FIN20QFF009	24.3%	19.1%	31.2%	9.0%	16.4%
FIN20QFF011	25.9%	12.4%	24.5%	14.6%	22.5%
FIN20QFF014	7.5%	16.8%	22.0%	23.0%	30.7%
FIN20QFF018	27.6%	13.5%	34.8%	12.3%	11.8%
FIN20QFF021	12.7%	23.4%	28.9%	18.6%	16.4%
FIN20QFF023	13.2%	22.7%	22.6%	17.3%	24.2%
FIN20QFF026	13.5%	25.6%	13.4%	21.4%	26.1%
FIN20QFF028	11.0%	22.6%	12.9%	25.2%	28.3%
FIN20QFF031	4.7%	31.8%	3.3%	29.1%	31.1%
FIN20QFF034	17.0%	29.0%	4.8%	33.1%	16.0%
FIN20QFF037	27.9%	21.9%	9.2%	21.3%	19.7%
FIN20QFF039	24.8%	20.4%	15.4%	20.0%	19.4%
FIN20QFF042	33.1%	24.1%	9.0%	15.0%	18.9%
FIN20QFF046	32.2%	16.3%	26.9%	14.3%	10.4%
FIN20QFF048	34.7%	16.7%	25.2%	9.0%	14.5%
FIN22QFF002	37.5%	16.9%	13.5%	12.9%	19.1%
FIN22QFF004	12.4%	16.8%	40.2%	19.6%	11.0%
FIN22QFF007	27.8%	11.7%	31.3%	17.7%	11.4%
FIN22QFF009	15.4%	9.7%	37.4%	20.5%	17.0%
FIN22QFF012	3.9%	11.9%	47.5%	23.1%	13.7%
FIN22QFF014	7.1%	14.2%	45.5%	20.0%	13.1%
Mean	19.5%	17.8%	28.0%	17.2%	17.6%

Table S6. Relative abundance (%) of selected BSOA-related fragment ions in factor MS profiles.

Ion	MO-OOA	BBOA-like	BSOA-like	CROA	HOA
$C_5H_6O^+$	0.174	0.146	0.348	0.369	0.048
$C_7H_9O_3^+$	0.015	0.010	0.107	0.137	0.079
$C_9H_{13}O_4^+$	0.011	0.006	0.020	0.018	0.018
$C_5H_7^+$	0.124	0.401	0.949	1.618	2.403
$C_6H_9^+$	0.000	0.186	0.310	0.590	1.474
$C_7H_7^+$	0.118	0.170	0.715	1.698	1.227

Table S7. Factor contributions (%) of selected BSOA-related fragment ions to their total mass.

Ion	MO-OOA	BBOA-like	BSOA-like	CROA	HOA
$C_5H_6O^+$	13.29	8.83	52.05	22.87	2.96
$C_7H_9O_3^+$	3.58	2.01	51.55	27.36	15.51
$C_9H_{13}O_4^+$	13.37	5.38	46.39	17.97	16.89
$C_5H_7^+$	2.25	5.76	33.53	23.73	34.73
$C_6H_9^+$	0.00	6.12	25.14	19.84	48.90
$C_7H_7^+$	2.94	3.38	34.86	34.35	24.47

Table S8. Distributions of ion families for measured WSOM spectra and those reconsulted from the spectra of HULIS and HP-WSOM.

Sample	Family	WSOM (%)	Reconstructed(%)	Difference （%）
FIN20Q002	CH	35.33	35.85	0.52
FIN20Q002	CHO1	36.23	36.98	0.75
FIN20Q002	CHO>1	19.31	18.17	-1.14
FIN20Q002	CHN	2.51	2.63	0.12
FIN20Q002	CHO1N	0.78	0.96	0.18
FIN20Q002	CHO>1N	0.55	0.53	-0.02
FIN20Q018	CH	29.65	32.70	3.04
FIN20Q018	CHO1	36.59	37.74	1.15
FIN20Q018	CHO>1	22.68	19.72	-2.95
FIN20Q018	CHN	2.93	2.79	-0.13
FIN20Q018	CHO1N	1.05	1.05	0.00
FIN20Q018	CHO>1N	0.52	0.49	-0.04

Crippa, M., Canonaco, F., Lanz, V. A., Äijälä, M., Allan, J. D., Carbone, S., Capes, G., Ceburnis, D., Dall'Osto, M., Day, D. A., DeCarlo, P. F., Ehn, M., Eriksson, A., Freney, E., Hildebrandt Ruiz, L., Hillamo, R., Jimenez, J. L., Junninen, H., Kiendler-Scharr, A., Kortelainen, A. M., Kulmala, M., Laaksonen, A., Mensah, A. A., Mohr, C., Nemitz, E., O'Dowd, C., Ovadnevaite, J., Pandis, S. N., Petäjä, T., Poulain, L., Saarikoski, S., Sellegri, K., Swietlicki, E., Tiitta, P., Worsnop, D. R., Baltensperger, U., and Prévôt, A. S. H.: Organic aerosol components derived from 25 AMS data sets across Europe using a consistent ME-2 based source apportionment approach, Atmos. Chem. Phys., 14, 6159-6176, https://doi.org/10.5194/acp-14-6159-2014, 2014.

Ulbrich, I., Canagaratna, M., Zhang, Q., Worsnop, D., and Jimenez, J.: Interpretation of organic components from Positive Matrix Factorization of aerosol mass spectrometric data, Atmospheric Chemistry and Physics, 9, 2891-2918, https://doi.org/10.5194/acp-9-2891-2009, 2009.

Ulbrich, I. M., Handschy, A., Lechner, M., and Jimenez, J.L: AMS Spectral Database [dataset],